JOURNAL OF THERMOPHYSICS AND HEAT TRANSFER
Vol. 12, No. 2, April–June 1998

Thermal Conductivity and Gaseous Microscale Transport

Mark Calvert* and John Baker†
University of Alabama in Birmingham, Birmingham, Alabama 35294

Previously, many numerical and analytical investigations into gaseous microscale flows have consisted of applying special boundary conditions to continuum-based formulations of the governing equations. These boundary conditions describe velocity slip and temperature jump conditions at solid/fluid interfaces for microscale flows. Noncontinuum effects within the flowfield interior are indirectly simulated by this approach, causing these formulations to become inaccurate with increasing rarefaction. A modified thermal conductivity relation has previously been shown to successfully model heat transfer through micron-sized gaps in areas such as insulations and contact regions. This paper reports results from an investigation that used this modified thermal conductivity approach in conjunction with continuum-based formulations of the governing equations to simulate pressure-driven, gaseous microscale flows. Comparisons against a traditional formulation for thermal conductivity in continuum-based governing equations indicate that use of modified thermal conductivity relations significantly affect the calculation of heat transport characteristics for gaseous microscale flows within the transition regime. Momentum transport characteristics do not show a similar trend. It is concluded that the use of thermophysical property models that transition from continuum to free molecular-based behavior is a viable approach to simulating microscale flows, and that further research in this area is needed.

Nomenclature

C = numerical constant
c_p = specific heat at constant pressure
c_v = specific heat at constant volume
L_c = characteristic length
M = molecular mass
p = pressure
q_c = heat conduction by Fourier's law
q_{FM} = free-molecular heat transfer
q_w = wall heat flux
R = gas constant
T = temperature
T_ϵ = characteristic of molecular force potential
u = velocity
x, y = spatial coordinates
γ = ratio of specific heats
κ = thermal conductivity
λ = molecular mean free path, $(\mu/\rho)\sqrt{\pi/(2RT)}$
μ = dynamic viscosity
ρ = density
σ = collision diameter of molecules
σ_v = specular reflection coefficient, momentum
σ_T = specular reflection coefficient, energy
τ_w = shear stress at the wall
Ω_v = collision integral

Dimensionless Parameters

C_f = friction factor, $\tau_w/(\rho u^2/2)$
C_h = Stanton number, $q_w/\rho u c_p(T_o - \bar{T})$
Kn = Knudsen number, λ/h
Pr = Prandtl number, $c_p\mu/k$

Subscripts

h = one-half of the microchannel height
N = noncontinuum
slip = slip conditions
wall = solid boundary conditions
0 = reference condition

Introduction

INTEREST in gaseous microscale flows has intensified over the last decade. Refinement of methodologies typically used to create integrated circuits has allowed the construction of mechanical components with characteristic lengths measured on the order of microns. This has begun a new area of technology called microelectromechanical systems (MEMS). This new technology has been used to manufacture devices such as actuators, sensors, compressors, and pumps with physical dimensions on the order of microns.[1,2] The technology associated with MEMS also has potential benefits far exceeding applications typically envisioned for microscale machines. By etching microchannels on the surfaces of integrated electronics, it is possible to increase the surface area for heat transfer without greatly increasing the size and weight of the components. These factors are extremely important, as are those associated with aerospace applications. The difficulty with gaseous microscale transport is that scaling laws traditionally applied in heat transfer and fluid dynamics do not capture the true behavior of transport in the microscale regime.[3] Rather than rarefaction effects being the result of reduction in density, microscale transport behavior results from a decrease in the length scales associated with the flowfield.

Pfahler et al.[4] first experimentally investigated gaseous flows through microchannels. They found that the friction coefficient for microscale flows decreased as rarefaction increased along the length of the microchannel, rather than remaining constant as in larger channels. This decrease was attributed to a decrease in effective viscosity caused by increasing noncontinuum effects. Ho and Tai[3] observed that the mass flow rate through microchannels was greater than would be expected from traditional, continuum-based fluid behavior. They also found that the pressure gradient along the length of the channel was nonlinear in nature. Experimental pressure data could only be graphically collapsed through nondimensionalization by use

Presented as Paper 97-0377 at the AIAA 35th Aerospace Sciences Meeting, Reno, NV, Jan. 6–9, 1997; received Aug. 18, 1997; revision received Nov. 25, 1997; accepted for publication Nov. 30, 1997.

*Graduate Student, Department of Materials and Mechanical Engineering, School of Engineering. Student Member AIAA.

†Assistant Professor, Department of Materials and Mechanical Engineering. E-mail: jbaker@eng.uab.edu. Member AIAA.

of a combined viscous-stress/length-based scale, implying that viscous forces have greater significance in microscale flows than inertial forces.

Arkillic and Breuer[5] analytically developed an expression for velocity distribution for pressure-driven, microscale Couette/Poiseuille flows in the slip-flow regime using first-order Maxwell velocity slip-boundary conditions. These boundary conditions have traditionally been used with the reduced pressure conditions associated with rarefied flows. This analytical expression assumed that gradients in thermal conductivity and viscosity were negligible within the flowfield. The analytical solution compared favorably with experimental data for microchannel flows. Further investigations[6,7] revealed that the nonlinearity of the pressure gradients along the length of a microchannel decreased with increasing rarefaction. Harley et al.[8] experimentally and numerically investigated compressible microchannel flows. They found that deviations of pressure normal to the flow direction were negligibly small. They also found that use of a first-order slip-boundary condition in their two-dimensional numerical model gave results that were in agreement with the experimental data for the slip-flow regime.

Beskok and Karniadakis[9] computationally and analytically investigated heat and momentum transfer characteristics of microscale flows. They used modified boundary conditions based on the Maxwell/Smoluchowski boundary conditions that were expanded higher-order terms in terms of a Knudsen number. The Knudsen number is defined as the ratio of the molecular mean free path to a characteristic length associated with the flowfield. Results indicated that heating of the microchannel reduced the volumetric flow rate. Further investigation revealed that increased Knudsen numbers reduced the nonlinearity of the pressure distribution in the microchannel and decreased compressibility effects. Their models gave favorable results in comparison with experimental data for rarefied flows through millimeter-sized channels.[10]

Calvert[11] used the Burnett equations to model microscale flows in the transition regime. The model used consisted of pressure-driven, microscale Poiseuille flows of helium between isothermal walls of differing temperatures. Results from test cases using these formulations revealed that the use of higher-order constitutive relations did not yield qualitative differences from the formulations that used the Navier–Stokes constitutive relations for flows with Knudsen numbers less than 1. The higher-order constitutive terms acted as minor corrections to the lower-order terms rather than representing any phenomenological behavior related to noncontinuum effects.

Previous investigations into the effects of noncontinuum conditions on thermophysical properties have focused on determining formulations to accurately predict conductive heat flux through microscale gaps. These modifications typically involved modifying the thermal conductivity to calculate an effective thermal conductivity for application in the area of insulations, typically for cryogenic applications. Smoluchowski first noted a decrease in thermal conduction with increasing rarefaction in granular insulators, which led to the derivation of the temperature-jump boundary condition.[12] Kistler[13] investigated the heat transfer through gas bubbles in silica aerogels. He assumed that all molecular interactions were with solid interfaces and developed a modified thermal conductivity that accounted for these effects. The actual heat flux was used to estimate the average size of bubbles within the aerogel. Verschoor and Greebler[14] investigated the thermal conduction through fibrous insulations. Like Kistler, they found that the normal thermal conductivity of the gas overestimated heat transfer by conduction. The reduction of heat transfer in the slip-flow and transition regimes because of noncontinuum effects was equivalent to the addition of a length of magnitude $[\Delta T/(\mathrm{d}T/\mathrm{d}n)]$ to the width between the solid walls for a fluid in the continuum regime.[12] Wesley and Yovanovich[15] found a similar relationship for gaseous gap heat conductance between the fuel and the clad of a nuclear fuel rod.

Noncontinuum effects on the apparent viscosity of fluids in the transition regime has been reported by Beenakker et al.[16] Using kinetic theory, they investigated molecular transport in nanometer channels where most or all molecular interactions are with the solid surface. They found that the presence of thermal gradients in the solid wall caused phonon–molecule interactions that produced a drag on the fluid in the direction of increasing temperature gradient. This effect was found to be inversely proportional to the square of the channel diameter. The authors noted that this effect might be noticeable in the micrometer range but would be insignificant in the millimeter range. No formulation of viscosity developed to account for this effect has been reported in the literature.

The focus of this research is to compare two different thermal conductivity formulations for modeling microscale transport. The first formulation examined will be a model using formulations of the Navier–Stokes x-momentum and energy equations with traditional formulations of thermal conductivity. The second formulation will use a modified thermal conductivity model that compensates for decreasing heat transfer because of gas rarefaction. These different formulations are outlined and the computational scheme used in this investigation is described. Details are presented as to solution convergence and validity when compared to experimental data. Comparisons will also be made between the different formulations in terms of velocity and temperature characteristics in the microchannel as well as comparisons of friction factor and Stanton number. Conclusions are then drawn from the results obtained in this investigation.

Formulation

The thermophysical properties of viscosity and thermal conductivity are measures of interactions between molecules within a fluid. Viscosity measures the intermolecular forces between molecules that cause fluids to resist shear. Thermal conductivity measures the ability of energetic molecules to transfer energy to molecules with less energy. These properties relate molecular interactions to macroscopic behavior. By relating these quantities to such macroscopic quantities as temperature and pressure, it is possible to treat fluids as a continuous distribution of matter without explicitly considering the discrete, molecular constituents. Formulations such as Sutherland's law and the power laws for viscosity and thermal conductivity relate these thermophysical properties of fluid to nonlinear functions of temperature. Molecular-force interactions are used to define numerical constants at characteristic temperatures. These formulations may then be used to extrapolate values for thermal conductivity and viscosity for temperature ranges around the characteristic temperature.

From the kinetic theory of gases, it is possible to derive expressions for thermal conductivity and viscosity that use molecular properties to compute values for these quantities. By considering the low density limit of gases, Chapman and Cowling[17] found that viscosity may be expressed as[18]

$$\mu = C_\mu(\sqrt{TM}/\sigma^2\Omega_v) \tag{1}$$

where C_μ has a value of 2.68×10^{-6} Å^2/(m·s)·(kmol·kg/K)$^{1/2}$. The low-density limit of a gas is defined as the region where ternary and greater molecular collisions may be neglected. At this limit, temperature has a much greater influence in determining viscosity and thermal conductivity than pressure. From a derivation similar to that used for viscosity, White[18] obtained an expression for thermal conductivity as

$$\kappa = C_\kappa[\sqrt{(T/M)}/\sigma^2\Omega_v] \tag{2}$$

where C_κ has a value of 8.33×10^{-2} Å^2·m/s^3·[(kg/K)^3/kmol]$^{1/2}$. These thermophysical property formulations were derived for

use with the SI system of units. The collision integral describes the approximate intermolecular force potential between molecules with a given effective collision diameter of σ. For noninteracting molecules, it attains a value of unity. From accepted theories for collision integrals, White developed a curve fit for the collision integral as

$$\Omega_v \approx 1.147(T/T_\epsilon)^{-0.145} + [(T/T_\epsilon) + 0.5]^{-2.0} \tag{3}$$

from existing data for the Stockmayer potential function.[18] T_ϵ is an effective temperature characteristic of the force potential and intermolecular forces between molecules of the gas. White found that the accuracy of the expression given by Eq. (3) lies within two percent of the existing data. The expressions for the viscosity and thermal conductivity may be manipulated to yield the more familiar forms of Sutherland's law and the power law for the respective thermophysical properties.

Heat conduction behavior in the transitional regime has been treated as an intermediate function of the asymptotic processes of continuum-based heat transfer and free-molecular heat transfer.[19] The continuum model is based on Fourier's law of heat conduction through a fluid. The free-molecular model calculates heat transfer by the number of molecules moving from a hot to cold surface, independent of the distance separating the two surfaces. This model assumes that the effect of intermolecular collisions is negligible. By using the Knudsen number to weight the contributions of the two models, an approximation to the true heat flux in the transitional regime is interpolated. This approach has been shown to agree well with experimental data for heat transfer through rarefied argon and helium. Sherman's interpolation formula[20] based on this approach is written as

$$q = \left(\frac{1}{q_{FM}} + \frac{1}{q_c}\right)^{-1} \tag{4}$$

where q_{FM} is defined as[21]

$$q_{FM} = -\frac{\sigma_T}{2 - \sigma_T}\frac{\gamma + 1}{\gamma - 1} p \sqrt{\frac{R}{8\pi T}}(T_h - T_{-h}) \tag{5}$$

for parallel walls. Assuming that the temperature difference divided by a characteristic length for the free molecular heat flux may be approximated as the temperature gradient of the continuum heat flux formulation, an expression for effective thermal conductivity may be derived as[21]

$$\kappa_N = \frac{\kappa}{1 + 2\dfrac{2 - \sigma_T}{\sigma_T}\dfrac{2\gamma}{\gamma + 1}\dfrac{\lambda/L_c}{Pr}} \tag{6}$$

This effective thermal conductivity is composed of the thermal gradient coefficients in the expression for heat flux given by Eq. (4). From inspection of this formulation, it may be noted that as the Knudsen number becomes small, the effective thermal conductivity approaches the thermal conductivity predicted by continuum-based formulations. As the Knudsen number becomes large, the heat flux approaches the free molecular values and the effective thermal conductivity approaches zero. It may be noted that this formulation requires use of the Prandtl number Pr, and the molecular mean free path λ. As these quantities are not independent of temperature and pressure, the definitions are substituted into Eq. (6) to yield

$$\kappa_N = \frac{1}{\left(\dfrac{1}{\kappa} + 2\dfrac{2 - \sigma_T}{\sigma_T}\dfrac{2\gamma}{\gamma + 1}\dfrac{1}{hC_p p}\sqrt{\dfrac{\pi RT}{2}}\right)} \tag{7}$$

Thus, this formulation is capable of simulating variations in the local effective thermal conductivity caused by the variation in noncontinuum-based behavior across the flowfield.

Model Problem

Consider pressure-driven Poiseuille flow as shown in the flow geometry model of Fig. 1. A linear pressure gradient is assumed in the x direction. Temperature and velocity are assumed to be functions of y only. The general x-momentum equation and energy equation for the model problem may be written as[11]

$$\frac{\partial p}{\partial x} + \frac{\partial \tau_{11}}{\partial x} + \frac{\partial \tau_{12}}{\partial y} = 0 \tag{8}$$

$$\frac{\partial q_1}{\partial x} + \frac{\partial q_2}{\partial y} + \tau_{12}\frac{\partial u}{\partial y} = 0 \tag{9}$$

Conservation of mass and y momentum was ensured during derivation of Eqs. (8) and (9) by substitution of the mass and y-momentum equations into the general x-momentum and energy equations.[11] Substituting the Navier–Stokes approximations for the shear-stress tensor and the heat flux vector and simplifying the resulting expressions yields the following governing equations for momentum and energy transport within the specified flowfield:

$$\frac{\partial p}{\partial x} - \frac{\partial \mu}{\partial y}\frac{\partial u}{\partial y} - \mu\frac{\partial^2 u}{\partial y^2} = 0 \tag{10}$$

$$\mu\left(\frac{\partial u}{\partial y}\right)^2 + \frac{\partial \kappa}{\partial y}\frac{\partial T}{\partial y} + \kappa\frac{\partial^2 T}{\partial y^2} = 0 \tag{11}$$

The decision to use a linear pressure distribution in the x direction was partially based on the observation that the nonlinearity of the pressure gradient decreases with increasing rarefaction.[10] The complexity of the model problem was also significantly reduced through assumption of a linear pressure distribution.

The Maxwell/Smoluchowski boundary conditions[22] for the model problem are given for $y = -h$ as

$$u = \lambda\frac{2 - \sigma_v}{\sigma_v}\left.\frac{du}{dy}\right|_{-h} \tag{12}$$

$$T = T_0 + \frac{\lambda}{Pr}\frac{2 - \sigma_t}{\sigma_t}\frac{2\gamma}{\gamma + 1}\left.\frac{dT}{dy}\right|_{-h} \tag{13}$$

and for $y = h$ as

$$u = -\lambda\frac{2 - \sigma_v}{\sigma_v}\left.\frac{du}{dy}\right|_{h} \tag{14}$$

$$T = T_1 - \frac{\lambda}{Pr}\frac{2 - \sigma_t}{\sigma_t}\frac{2\gamma}{\gamma + 1}\left.\frac{dT}{dy}\right|_{h} \tag{15}$$

The thermal creep component has been removed from the velocity boundary conditions through the assumption of isother-

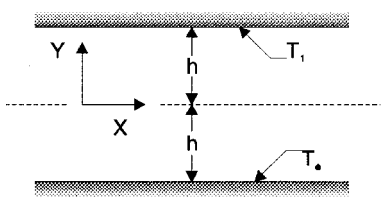

Fig. 1 Schematic of the flow geometry.

mal walls. This condition was applied for the purpose of validation with previously published results. The difference in signs for the derivative at the upper and lower walls is a result of the direction of the vector normal to those walls. In this paper, the assumption of unity for both accommodation coefficients has been justified based on information found in Steinheil et al.[23]

For numerical solution, the governing equations were discretized through the use of second-order-accurate, finite difference formulas. Center difference formulas were substituted for the derivatives in the governing equations. The discretized Maxwell/Smolushowski boundary conditions were used to define image points beyond the solid interfaces. These image points were then used in the governing equations for points on the boundaries. The preceding formulation resulted in a set of nonlinear differential equations. Solutions for these equations were obtained by Picard iteration on the linear terms of the governing equations while lagging the nonlinear thermophysical property formulation values. This allowed the set of equations to be solved in tridiagonal form. This process was continued until the successive solutions for velocity and temperature converged to a tolerance near machine precision. For the cases where noncontinuum effects on thermophysical properties were investigated, the effective thermal conductivity κ_N was substituted for the traditional κ in the energy equation.

Results

Prior to running numerical experiments, a grid function convergence test was undertaken to determine an optimum grid spacing that would ensure grid independence in the solutions. By comparing the results of a series of successively finer grids, it was found that second-order accurate results were obtained for both thermal conductivity property model formulations with 201 grid points across a microchannel of 1.33 μm for the largest temperature and pressure gradients investigated. Thus, 201 grid points were used for all cases presented in this paper.

Additional tests were also performed to examine the solution stability of the numerical formulations used in this investigation. The solution convergence was checked by varying the initial approximations to the correct solutions in the iterative process. No quantitative differences were observed between the solutions for the different initialization sets. Also, the use of relaxation factors in the iterative solution process did not cause any quantifiable differences in the solution sets. The results from these tests were felt to be sufficient to guarantee convergence to a unique solution.

Table 1 lists the default parameters for the cases run in this investigation. Quantities that were varied during the numerical experiments discussed here are explicitly shown on the plots or are stated in the related text. Helium was used as the working fluid for this investigation because of its monatomic nature and the close association of its property values with those of an ideal gas. The temperature of the bottom wall was used as the reference temperature T_0. ΔT was defined as the temperate difference between the top wall and the bottom wall; negative values indicate a cooler top wall than the lower wall.

For validation purposes, experimental mass flow rate data, from Arkillic et al.,[7] were used to assess the accuracy of the Navier–Stokes formulation. Note that there are several differences between the flows studied in the numerical simulations and the experiment. The first is the fact that the simulation formulations are based on governing equations derived for a two-dimensional Poiseuille flow. Three-dimensional effects are not considered by the numerical formulations presented here. The second difference is that the total pressure drop from microchannel inlet to outlet divided by the total channel length from the experiments was used to define the local pressure gradients for the numerical simulations. The experimental apparatus was not instrumented to provide data on the pressure distribution along the length of the microchannel. While Beskok et al.[10] observed that increasing rarefaction effects appeared to decrease deviation from a linear pressure gradient in microscale flows, the nonlinearity of the pressure gradient along the total length of the microchannel may not be small enough to be considered negligible, particularly with increasing pressure ratios, for the rarefied flows considered here (Kn = 0.165). A graph of the simulation results vs the experimental data is given in Fig. 2. Relevant parameters for the validation simulation are given in Table 2. From this graph, it is seen that all of the simulation results are uniformly larger than the experimental results. It may also be observed that the difference between the experimental results and the simulation results increases with increasing pressure ratio. Despite these factors, the numerical simulations agree within 5% of the experimental data. Because of this, the numerical formulations were felt to be validated by the experimental data. The plots of the various formulations considered here are indistinguishably close.

Additionally, the code was validated by comparison with analytical solutions for the momentum and energy equations. The solutions were obtained by assuming that gradients in viscosity and thermal conductivity terms were negligibly small. By making this assumption, Eqs. (10) and (11) could be written as

$$\frac{\partial p}{\partial x} - \mu \frac{\partial^2 u}{\partial y^2} = 0 \tag{16}$$

$$\mu \left(\frac{\partial u}{\partial y}\right)^2 + \kappa \frac{\partial^2 T}{\partial y^2} = 0 \tag{17}$$

Table 1 Default parameters for the test cases

Kn	0.165	dp/dx	−1000 kPa/m
Pr	2/3	ΔT	−100.0 K
σ	2.551 Å	T_0	314 K
γ	5/3	T_ϵ	0.7173 K
M	4.003	——	——

Table 2 Properties for validation simulations

Property	Value
One-half channel height, h	0.665 μm
Channel width, w	52.25 μm
Knudsen number, Kn	0.165
Number of grid points, N	201
Specular reflection coefficient, σ_T, σ_v	1
Temperature of lower wall, $T_{w,h}$	314 K
Temperature of upper wall, $T_{w,h}$	314 K

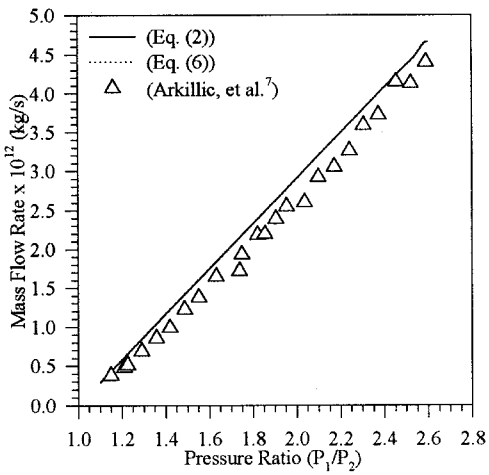

Fig. 2 Results for validation simulations.

Using the Maxwell/Smoluchowski boundary conditions and assumptions given previously, Eqs. (16) and (17) could be solved as ordinary, second-order differential equations to yield

$$u(y) = \frac{1}{2\mu}\frac{\partial p}{\partial x}\left(y^2 - h^2 - 2\frac{2-\sigma_v}{\sigma_v}\lambda h\right) \tag{18}$$

$$T(y) = \frac{1}{12\mu\kappa}\left(\frac{\partial p}{\partial x}\right)^2\left(y^4 - h^4 - 4\frac{2-\sigma_T}{\sigma_T}\frac{2\gamma}{\gamma+1}\frac{\lambda}{Pr}h^3\right) + \frac{T_{w,h} - T_{w,-h}}{2\left(h + \frac{2-\sigma_T}{\sigma_T}\frac{2\gamma}{\gamma+1}\frac{\lambda}{Pr}\right)}y + \frac{T_{w,h} + T_{w,-h}}{2} \tag{19}$$

Arkilic and Breuer[5] and Beskok and Karniadakis[9] validated similar solutions up to the edge of the slip-flow regime near the transition regime. Comparison of the numerical solutions to the analytical solutions did not reveal any discernible differences over the range of applicability of the analytical solutions for the traditional thermal conductivity test cases. The temperature solutions for the noncontinuum thermal conductivity test cases did deviate slightly for the largest Knudsen numbers investigated in the comparison, though the deviation was less than 1%. Thus, the numerical formulations were assumed to be validated over the continuum and slip-flow regimes.

Figure 3 shows values of thermal conductivity as a function of temperature and Knudsen number for the true thermal conductivity and effective thermal conductivity formulations. As may be seen from Fig. 3, all cases of thermal conductivity increase with increasing temperature. It may be noted, however, that the rate of increase decreases slightly with increasing temperature for the true thermal conductivity and the effective thermal conductivity for $Kn = 10^{-3}$. However, increasing Knudsen numbers decreases this nonlinearity. For the larger Knudsen number cases investigated, effective thermal conductivity was proportional to temperature. The effective thermal conductivity decreased with increasing Knudsen numbers. Figure 4 shows effective thermal conductivity normalized by the true thermal conductivity as a function of Knudsen numbers for a temperature of 323 K. As may be seen from the plot, effective thermal conductivity is a nonlinear function of Knudsen numbers.

Figures 5 and 6 show plots for the friction and Stanton numbers as functions of Knudsen numbers and pressure gradients, respectively. The pressure gradient was increased by an order of magnitude from -10^5 to -10^8 Pa/m. Each increase in magnitude of the pressure gradient resulted in a proportional decrease in friction factor and Stanton number for the range of Knudsen numbers shown. The friction factor and Stanton number showed similar behavior as Knudsen numbers increased from 10^{-3} to 10^{-2}. For Knudsen numbers above 10^{-2}, the rates of decrease for the Stanton number and friction factor as functions of Knudsen numbers increased in a nonlinear fashion for increasing Knudsen numbers. It may be observed from Fig. 6 that the rate of decrease in Stanton number is greater for the effective thermal conductivity formulations than it is for the traditional thermal conductivity relations for Knudsen numbers

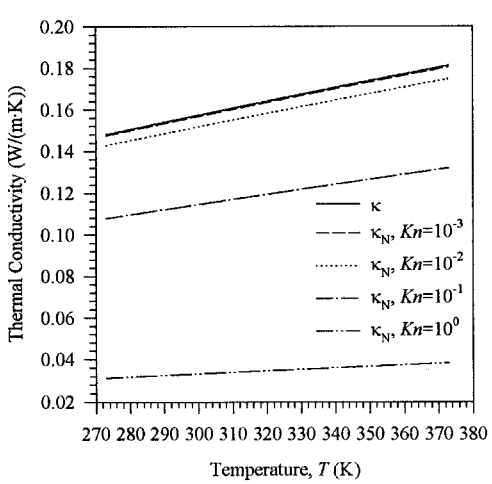

Fig. 3 Thermal conductivity as a function of temperature.

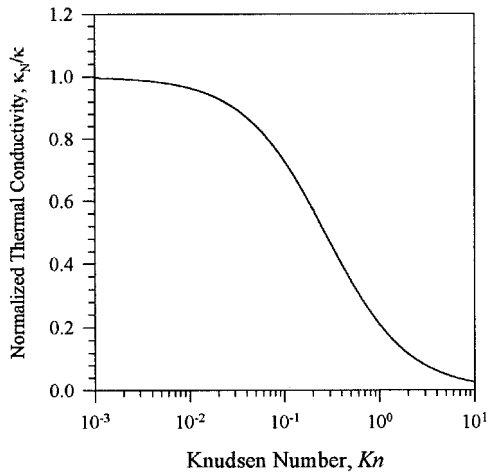

Fig. 4 Normalized effective thermal conductivity as a function of Knudsen number.

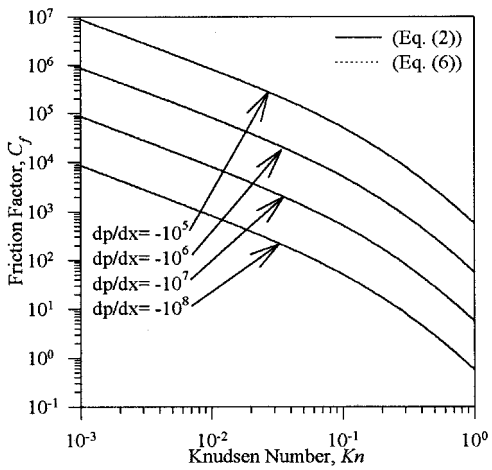

Fig. 5 Friction factor as function of pressure gradient and Knudsen number.

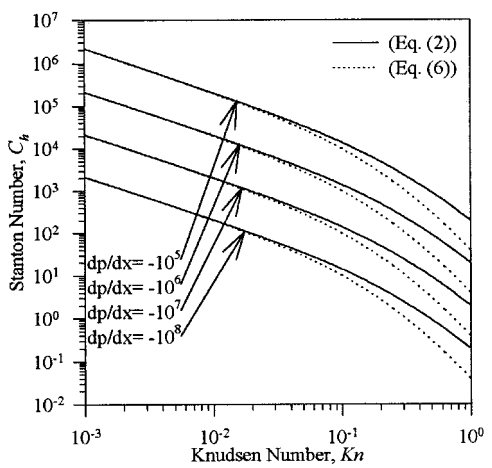

Fig. 6 Stanton number as function of pressure gradient and Knudsen number.

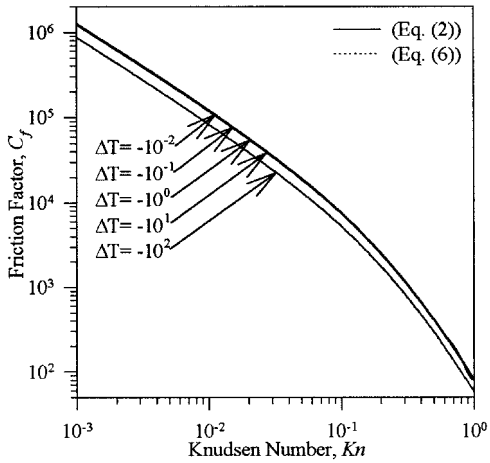

Fig. 7 Friction factor as function of temperature difference and Knudsen number.

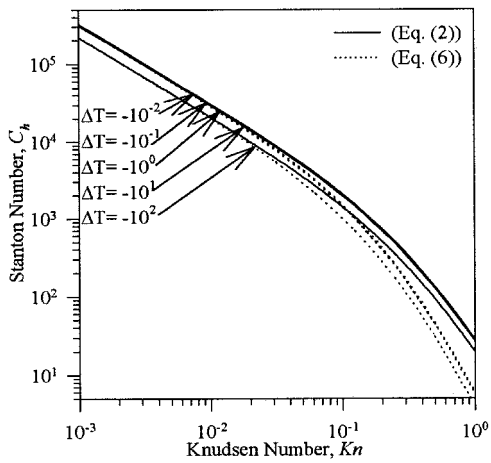

Fig. 8 Stanton number as function of temperature difference and Knudsen number.

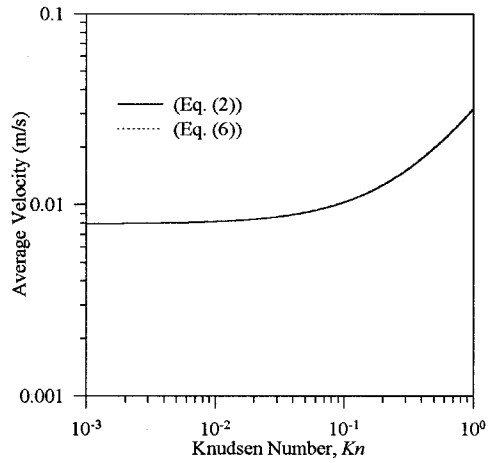

Fig. 9 Average velocity as function of Knudsen number.

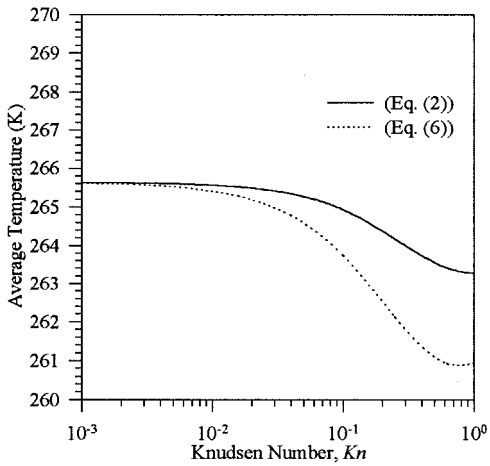

Fig. 10 Average temperature as function of Knudsen number.

greater than 10^{-2}. The plots of friction factor do not exhibit this behavior, however.

Figures 7 and 8 show graphs of the friction factor and Stanton number as functions of temperature differences between the upper and lower surfaces and Knudsen numbers. As may be observed from the plots, neither friction factor nor Stanton number are noticeably affected as the magnitude of the temperature difference is increased from 10^{-2} to 10^{1}. When the magnitude of the temperature difference is increased from 10^{1} to 10^{2}, the friction factor and Stanton number decrease by approximately 36 and 66%, respectively, for Knudsen numbers less than 10^{-2}. For Knudsen numbers above this point, the differences between the profiles decrease until they reach values of approximately 29% for the friction factor and 18% for the Stanton number at $Kn = 1$. This would seem to indicate that increasing rarefaction effects tend to mitigate temperature gradients within the fluid. This is further illustrated by the decrease in the friction factor and Stanton number with increasing Knudsen numbers. The rate of decrease increases in a nonlinear manner above $Kn = 0.01$ as noncontinuum effects become more significant in determining fluid behavior. This would seem to be as intuitively obvious as it would be expected that the temperature of the fluid across the channel would reach an average profile with increasing rarefaction effects. As seen in Figs. 6 and 8, the use of the modified thermal conductivity formulations produced Stanton numbers that were smaller than those obtained with traditional formulations for Knudsen numbers greater than 10^{-2}. For $Kn = 1$, the Stanton numbers differed by approximately 140%. Again, the friction factor was not significantly affected by the use of the effective thermophysical properties. The plots for the two thermophysical formulations lie indistinguishably close as shown on Figs. 5 and 7.

Figures 9 and 10 show average velocity and temperature across the flowfield as the Knudsen number is increased from 10^{-3} to 1. As may be observed from Fig. 9, average velocity was not significantly influenced by variation of the thermal conductivity models. The average velocity within the flowfield remains fairly constant for Knudsen numbers less than 10^{-2}, by increases exponentially above that point. The average temperature does show a dependence on the thermophysical property model. The traditional thermal conductivity formulation remains fairly constant at 265.6 K for Knudsen numbers less than 10^{-2}, after which point it decreases until it reaches a value of 263.2 K. The effective thermal conductivity formulation exhibits a small rate of decrease until $Kn = 10^{-2}$, after which point the rate of decrease increases until approximately $Kn = 0.6$, after which it attains a value of approximately 261 K. This reduction would appear to be physically reasonable as heat conduction and viscous dissipation would be expected to decrease with increasing noncontinuum effects.

Figure 11 shows the temperature jump conditions at the upper and lower walls. From comparison with Fig. 10, it may be seen that the temperature difference between the temperature of the fluid at the boundary and the average temperature remains approximately equal for the traditional and effective thermal conductivity formulations. It may also be noted that this difference decreases with increasing Knudsen numbers. From this behavior and that exhibited by average velocity as a function of Knudsen numbers, it may be observed that in-

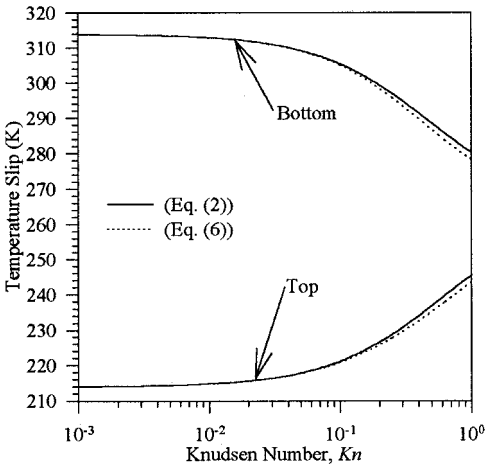

Fig. 11 Temperature slip as function of Knudsen number.

creasing noncontinuum effects result in a decrease in heat flux per unit volume of fluid per unit time. This indicates reduced thermal transport capabilities for microscale flows in the transition regime, as would be expected.

From Figs. 10 and 11, it may be seen that the use of the modified thermal conductivity relation does not cause a significant change in magnitude in the difference between the average temperature of the fluid and the temperature of the fluid immediately adjacent to a boundary when compared to the case for the traditional thermal conductivity relation. However, Figs. 6 and 8 show a significant difference between the plots for a Stanton number using the traditional and effective thermal conductivity relations for the largest Knudsen numbers investigated. This reveals that the formulation for thermal conductivity relation can be the most significant factor in describing the thermal transport characteristics of microscale flows.

From the behavior exhibited by the noncontinuum thermal conductivity formulation plots, it is seen that the use of a weighting function based on Knudsen numbers has the effect of causing a decrease in thermal conduction at the microscale levels. The reason for this is the significance of molecular-surface interactions in comparison to pure molecular interactions. The derivation of the traditional formulation for thermal conductivity does not explicitly consider the possibility that the number of molecule-surface collisions could be of the same order as molecule–molecule collisions. By this, the thermal conduction coefficient used in continuum-based flows could be viewed as the maximum thermal conduction capacity of the fluid. The possibility of the fluid achieving this maximum increases with the number of molecular collisions. However, in microscale geometries, surface effects dominate molecular collisions, causing thermal transport interactions between solid surfaces and molecules to predominantly govern thermal conduction.

Conclusions

From the results presented here, it is seen that modification of the thermal conductivity has a significant impact on predicted heat transport by microscale flows. Increasing rarefaction causes a decrease in heat flux per unit volume of fluid. Results from the effective thermal conductivity models indicate that traditional formulations of thermal conductivity underestimate this phenomenon. It was shown that the decrease in the effective conductivity with increasing Knudsen number was significant when compared to equivalent values from the traditional thermal conductivity formulation. However, the effective thermal conductivity does not significantly affect momentum transport by the fluid. The differences in temperature predicted by the modified model and the traditional model did not cause a significant change in viscosity that would noticeably affect the flow behavior.

The lack of any appreciable influence on momentum transport reveals a need for further research in thermophysical property models for microscale flows. Research in free-molecular flows has shown that fluids exhibit viscous behavior that would not be expected from calculations involving traditional formulations of thermophysical properties. However, results obtained from use of an effective thermal conductivity does not reveal this trend for momentum transport with increasing Knudsen numbers as it does for thermal transport. This would seem to indicate that further research is needed in the area to develop a formulation for effective viscosity equivalent to that of thermal conductivity. As such, the formulation for effective viscosity would serve to asymptotically transition from continuum viscous behavior to free-molecular viscous behavior. The development of such a formulation should effectively extend the range of applicability of the Navier–Stokes equations into the transition regime.

Acknowledgment

This research has been made possible by NASA Training Grant NGT-40010 from NASA and the Alabama Space Grant Consortium.

References

[1]Mehregany, M., DeAnna, R. G., and Reshotko, E., "Microelectromechanical Systems for Aerodynamics Applications," AIAA Paper 96-0421, Jan. 1996.

[2]Vargo, S. E., and Muntz, E. P., "A Simple Micromechanical Compressor and Vacuum Pump for Flow Control and Other Distributed Applications," AIAA Paper 96-0310, Jan. 1996.

[3]Ho, C. M., and Tai, Y. C., "MEMS: Science and Technology," *Application of Microfabrication to Fluid Mechanics*, American Society of Mechanical Engineers, FED, Vol. 197, New York, 1994, pp. 39–49.

[4]Pfahler, J., Harley, J., Bau, H., and Zemel, J. N., "Gas and Liquid Flow in Small Channels," *Micromechanical Sensors, Actuators and Systems*, American Society of Mechanical Engineers, DCS, Vol. 32, New York, 1991, pp. 49–60.

[5]Arkillic, E. B., and Breuer, K. S., "Gaseous Flow in Small Channels," AIAA Paper 93-3270, July 1993.

[6]Arkillic, E. B., Breuer, K. S., and Schmidt, M. A., "Gaseous Flow in Microchannels," *Application of Microfabrication to Fluid Mechanics*, American Society of Mechanical Engineers, FED-Vol. 197, New York, 1994, pp. 57–66.

[7]Arkillic, E. B., Schmidt, M. A., and Breuer, K. S., "Gaseous Slip Flow in Long Microchannels," *Journal of Microelectromechanical Systems*, Vol. 6, No. 2, 1997, pp. 167–178.

[8]Harley, J. C., Huang, Y., Bau, H. M., and Zemel, J. N., "Gas Flow in MicroChannels," *Journal of Fluid Mechanics*, Vol. 284, 1995, pp. 257–274.

[9]Beskok, A., and Karniadakis, G. E., "Simulation of Heat and Momentum Transfer in Complex Microgeometries," *Journal of Thermophysics and Heat Transfer*, Vol. 8, No. 4, 1994, pp. 647–655.

[10]Beskok, A., Karniadakis, G. E., and Trimmer, W., "Rarefaction, Compressibility and Thermal Creep Effects in Micro-Flows," American Society of Mechanical Engineers, Intersociety Energy Conversion Engineering Conf., San Francisco, CA, 1995.

[11]Calvert, M. E., "Analysis of Microscale, Transitional Regime Flow Using Burnett Relations," M.S. Thesis, Dept. of Material and Mechanical Engineering, Univ. of Alabama, Birmingham, AL, 1997.

[12]Kaganer, M. G., *Thermal Insulation in Cryogenic Engineering*, Israel Program for Scientific Translations, Ltd., Jerusalem, Israel, 1969.

[13]Kistler, S. S., "The Relation Between Heat Conductivity and Structure in Silica Aerogel," *Journal of Physical Chemistry*, Vol. 39, No. 1, 1934, pp. 79–85.

[14]Verschoor, J. D., and Greebler, P., "Heat Transfer by Gas Conduction and Radiation in Fibrous Insulations," *Transactions of the American Society of Mechanical Engineers*, Vol. 74, Aug. 1952, pp. 961–968.

[15]Wesley, D. A., and Yovanovich, M. M., "A New Gaseous Gap Conductance Relationship," *Nuclear Technology*, Vol. 72, Jan. 1986, pp. 72–74.

[16]Beenakker, J. J. M., Borman, V. D., and Krylov, S. Y., "Molecular Transport in the Nanometer Regime," *Physical Review Letters*, Vol. 72, No. 4, 1994, pp. 514–517.

[17]Chapman, S., and Cowling, T. G., *The Mathematical Theory of*

Non-Uniform Gases, 3rd ed., Cambridge Univ. Press, Cambridge, England, UK, 1970.

[18]White, F. M., "1-3, Properties of a Fluid," *Viscous Fluid Flow*, 2nd ed., McGraw–Hill, New York, 1991, pp. 15–45.

[19]Springer, G. S., "Heat Transfer in Rarefied Gases," *Advances in Heat Transfer*, Vol. 7, 1971, pp. 163–218.

[20]Sherman, F. S., "A Survey of Experimental Results and Methods for the Transition Regime of Rarefied Gas Dynamics," *Rarefied Gas Dynamics*, edited by J. A. Lauermann, Vol. 2, Academic, New York, 1963, pp. 228–260.

[21]Gephart, B., "Composite Transport Regions," *Heat Conduction and Mass Diffusion*, 1st ed., McGraw–Hill, New York, 1993, pp. 399–456.

[22]Burmeister, L. C., *Convective Heat Transfer*, Wiley, New York, 1983, Chap. 3.

[23]Steinheil, E., Scherber, W., Seidl, M., and Rieger, H., "Investigation on the Interaction of Gases and Well-Defined Solid Surfaces with Respect to Possibilities for Reduction of Aerodynamic Friction and Aerodynamic Heating," *Rarefied Gas Dynamics*, edited by J. Potter, Vol. 51, Pt. 1, 1976, pp. 589–602.